J Mater Sci (2010) 45:5089–5093
DOI 10.1007/s10853-010-4468-6

ICAM 2009

Intragranular formation of austenite during delta ferrite decomposition in a duplex stainless steel

Eduardo Franco de Monlevade · Helio Goldenstein · Ivan Gilberto Sandoval Falleiros

Received: 1 December 2009 / Accepted: 3 April 2010 / Published online: 16 April 2010

Abstract A Fe–22.5%Cr–4.53%Ni–3.0%Mo duplex stainless steel was solution treated at 1,325 °C for 1 h, quenched in water and isothermally treated at 900 °C for 5,000 s. The crystallography of austenite was studied using EBSD technique. Intragranular austenite particles formed from delta ferrite are shown to nucleate on inclusions, and to be subdivided in twin-related sub-particles. Intragranular austenite appears to have planar-only orientation relationships with the ferrite matrix, close to Kurdjumov–Sachs and Nishyiama–Wassermann, but not related to a conjugate direction. Samples treated at 900 °C underwent sparse formation of sigma phase and pronounced growth of elongated austenite particles, very similar to acicular ferrite.

Introduction

Duplex stainless steels are a grade of steels that presents approximately the same quantities of austenite and ferrite. These steels, in the absence of brittle intermetallic phases, tend to present higher mechanical resistance than austenitic or ferritic steels, as well as a better corrosion resistance. The occurrence of austenite at low temperatures make these steels a good model for studying crystallographic and morphological aspects of the austenite–ferrite transformation [1], as it avoids the need to calculate the austenite crystallography from that of martensite.

E. F. de Monlevade (✉) · H. Goldenstein · I. G. S. Falleiros
Departamento de Engenharia Metalúrgica e de Materiais, Escola Politécnica da Universidade de São Paulo, Avenida Professor Mello Morais, 2463, São Paulo, SP 05508-900, Brazil
e-mail: efmonlevade@uol.com.br; eduardo.monlevade@gmail.com

As far as elongated (plate-like or needle-like, which is normally not possible to determine in cross-sections) products are concerned in ferrous alloys, there are two possible structures that can be formed in the formation of austenite: Widmanstätten and acicular, the difference being that Widmanstätten particles are nucleated on grain boundaries or formed from grain boundary allotriomorphs, while acicular austenite is nucleated in the interior of the grain. Most of the work on this kind of structure, however, has been done in the eutectoid decomposition of austenite in carbon and low alloy steels.

Yokomiso et al. [2] performed a three-dimensional reconstruction study of intragranular ferrite, and reported that the three-dimensional shape of those particles is quite more irregular than the two-dimensional cross-section analyses suggest. They also point out that inclusions are the nucleation sites for intragranular ferrite particles, and that these particles are often composed of several different crystals, and most of them are in contact with the inclusions. Spanos et al. [3] performed EBSD analyses of early stages of formation of Widmanstätten ferrite from grain boundaries and grain boundary allotriomorphs. The authors also mention that secondary Widmanstätten branches are composed of several misoriented crystals containing ferrite:ferrite boundaries (indicating sympathetic nucleation of ferrite during growth of elongated particles), and that they appear to approach a common orientation as they extend into the austenite grain. In this regard, Shek et al. [4], in a study of early stages of formation of Widmanstätten ferrite in duplex stainless steels, reported that the ferrite nucleates at the grain boundaries holding ORs close to the Young–Kurdjumov–Sachs and Nishyiama–Wasserman. These precipitates tend to have an increasingly closer to exact YKS orientation relationships as the particle tip gets farther from the allotriomorph from which it derives.

Experimental procedures

The steel used in this study was a SAF2205 (UNS31803) type duplex stainless steel provided by Villares Metals. The chemical composition is given in Table 1. Samples 1 cm^3 in size were solution treated for 1 h in air at 1,325 °C and water quenched. Samples were further submitted to isothermal heat treatments at 900 °C for 5,000 s (1 h 23 min). The samples were sectioned and polished down to 1-μm diamond using standard metallographic procedures. Etching was done using the tint etch described by Beraha and Shpigler [5]. Samples were observed using optical and scanning electron microscopy, and also submitted to electron back-scattering diffraction (EBSD) for crystallographic analyses. Scanning electron microscopy and EBSD were conducted in a FEI XL-30 thermal emission gun SEM, equipped with a TexSem Laboratories (TSL) EBSD system. As a final preparation step for EBSD, samples were polished in colloidal silica and etched in a 30% volume hydrochloric acid solution for microstructure delineation. The recipe for both reagents used is shown in Table 2. Orientation relationships between austenite precipitates and the ferrite matrix were obtained by graphical and algebraic methods. The algebraic method is based on the use of Bunge's [6] orientation matrix to calculate the misorientation between the austenite and ferrite crystals. This is particularly straightforward with relations between cubic crystals, as both are represented by orthonormal reference systems. The algebraic calculation of the orientation relationships yields a unequivocal determination of the planes involved in the ORs. The experimental error in the determination of orientation relationships using the EBSD technique is estimated to be of approximately ±2 degrees.

Table 1 Chemical composition of the steel used in this study

C	Si	Mn	P	S	Co	Cr
0.016	0.66	0.62	0.009	0.0016	0.030	22.60
Mo	Ni	V	Cu	Al	B	N
3.06	4.73	0.02	0.07	0.013	0.0031	0.20

Results and discussion

The microstructure obtained after solution treatment and water quench is shown in Fig. 1. During the solution treatment, extensive growth of the ferrite grains took place. Upon quenching, austenite was formed on the grain

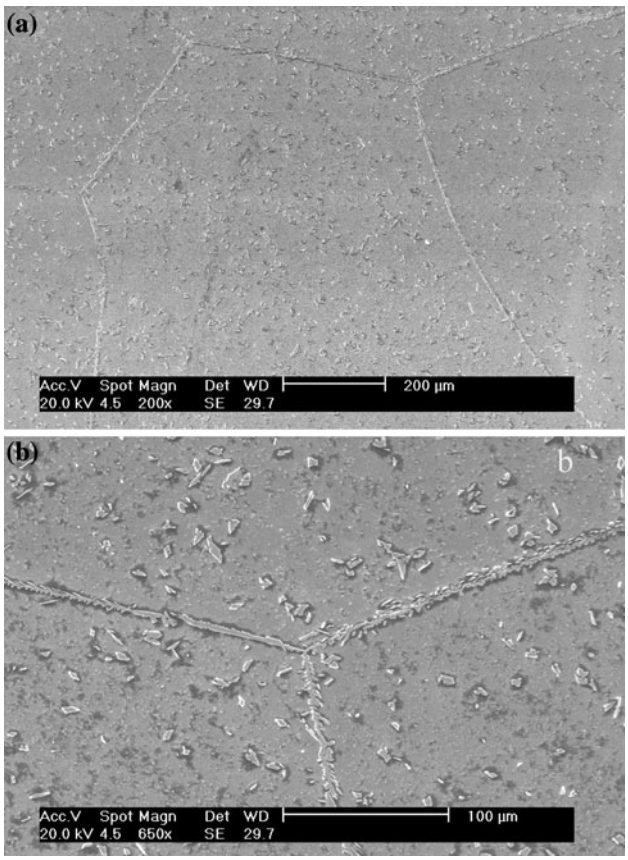

Fig. 1 As quenched structure: large ferrite grains, with austenite formed on grain boundaries and inside the grains, and chromium nitrides disperse in the ferrite matrix; **a** general view; **b** detail view of a triple grain boundary junction

Table 2 Etchants used in this study and their effects

Etchant	Composition	Effect
Beraha's tint etch for stainless steels	70 mL distilled water	Ferrite is brown or blue (depending on orientation and thickness of the deposited film);
	30 mL hydrochloric acid (HCl)	Austenite is lightly etched (slightly yellow)
	1–2 g postassium metabissulfite ($K_2S_2O_5$) for each 100 mL of solution	Sigma remains unetched
Hydrochloric acid	70 mL distilled water	Ferrite turns light brown
	30 mL hydrochloric acid (HCl)	Austenite is lightly etched (slightly yellow)
		Sigma remains unetched

boundaries and also in the interior of the grains. The crystallography of the grain boundary austenite was studied in a previous work by two of the present authors [7]. The extensively formed rod-like particles are chromium nitrides precipitated due to the large supersaturation of nitrogen in the ferrite matrix. The surroundings of austenite particles, however, are free of nitrides, indicating that the austenite formation during quenching was controlled by nitrogen diffusion into the newly formed austenitic particles.

An EBSD analysis of a region containing grain boundary austenite and intragranular austenite and a cluster of intragranular austenite formed during quench is shown in Fig. 2. A cropped section from that analysis is shown in Fig. 3. This cluster is shown to be composed of austenite

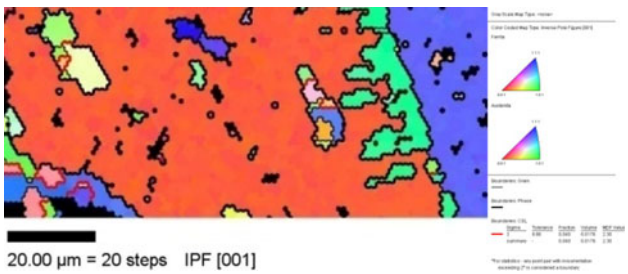

Fig. 2 EBSD analysis of a region containing grain boundary austenite and intergranular clusters of austenite

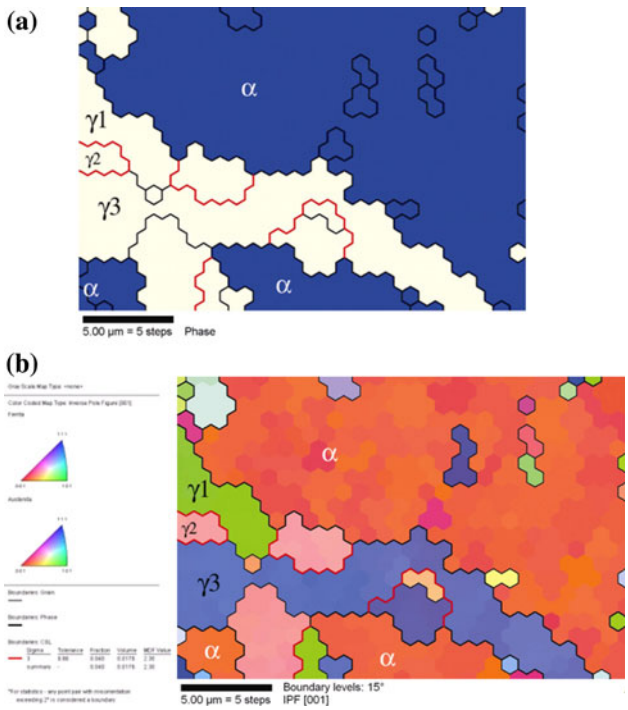

Fig. 3 EBSD analysis of intragranular austenite cluster: boundaries marked in *grey* (*red* in color version) are twin boundaries, defined by a Σ3 coincidence lattice constant; **a** phase identification (austenite is *white*); **b** orientation map

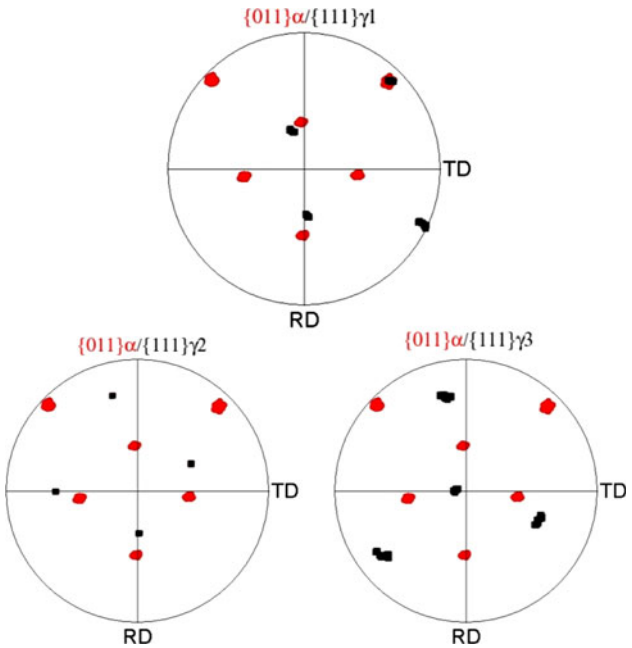

Fig. 4 {111} stereographic projections of austenite overlaid to the {110} projection of the ferrite matrix. Only $\gamma 1$ holds an orientation relationship with the ferrite matrix

crystals that bear a twinning relation between each other. The graphical analysis of the orientation relationships between the austenite cluster and the ferrite matrix is shown in Fig. 4. It was identified that only the austenite particle labeled $\gamma 1$ in Fig. 2 holds an orientation relationship with the matrix, which suggests that this is the first nucleating crystal. The austenite labeled $\gamma 2$ in Fig. 2 has a twinning relationship to $\gamma 1$, and the particle labeled $\gamma 3$ in Fig. 2, in turn, holds a twin relationship to $\gamma 2$. In both $\gamma 2$ and $\gamma 3$, one {111} plane (the twinning plane between them) holds a misorientation close to 60° from the {011} plane in the ferrite matrix directly involved in the orientation relationship with $\gamma 1$. The graphic analysis of the crystallographic relations between austenite particles in the cluster shown in Figs. 3 and 5. The calculated orientation relationships are shown in Table 3. This sort of cyclic or sequential twinning phenomenon is also observed in other systems, such as tin-based alloys used in electronics. Some solder spheres, upon solidification, tend to undergo cyclic twinning, which gives rise to a structure known as "Kara's Beach Ball" [8] (named after its discoverer). A beach ball structure was observed and reported by Lehman et al. [9] (this structure is depicted in Ref. 9, Fig. 12d). The microstructure depicted in Ref. 9 was revealed using polarized light that yields different responses from the tetragonal structure of tin according to its orientation. It should be noticed that opposite crystals share the same orientation, both in the structure observed in tin and in the case presented in this article. In this way, it may be possible to state

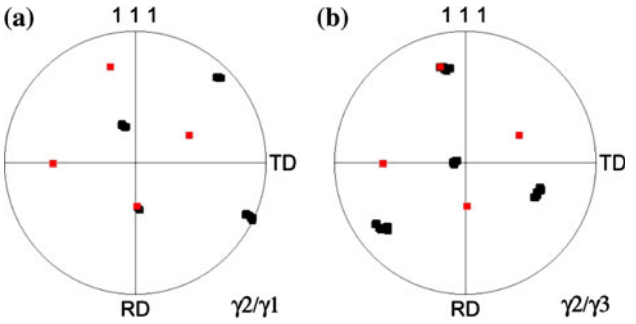

Fig. 5 Orientation relationships between austenite particles within a same cluster; **a** overlap of the {111} stereographic projections of $\gamma 1$ (in *black*) and $\gamma 2$, showing a twin relation between them; **b** overlap of the {111} stereographic projections of $\gamma 3$ (in *black*) and $\gamma 2$, showing a twin relation

Table 3 Calculated orientation relationships between austenite and ferrite in the cluster shown in Fig. 3

Crystals	Orientation relationships	
$\gamma 1/\alpha$	$(1\bar{1}1)\gamma \xrightarrow{0^\circ} (1\bar{1}0)\alpha$	$[10\bar{1}]\gamma \xrightarrow{1^\circ} [11\bar{1}]\alpha$
$\gamma 2/\alpha$	$(111)\gamma \xrightarrow{57^\circ} (1\bar{1}0)\alpha$	No low angle relationship with α
$\gamma 3/\alpha$	$(11\bar{1})\gamma \xrightarrow{57^\circ} (1\bar{1}0)\alpha$	

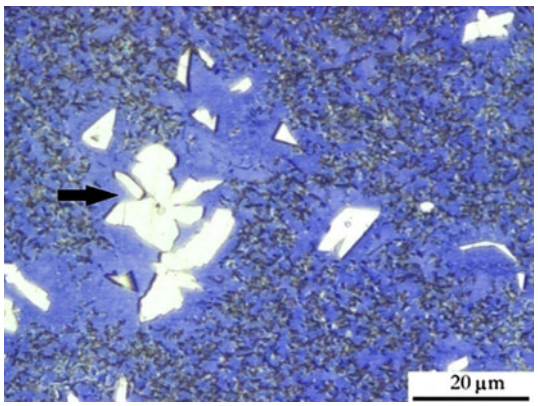

Fig. 6 Intragranular austenite cluster nucleated on an inclusion (pointed by the *black arrow*). This cluster is similar to the one shown in Figs. 2, 3

that there is a tendency for the formation of "flat beach ball" structures in austenite formation from ferrite during fast cooling. Also, these results are similar to those obtained by Yokomiso et al. [2] studying intragranular ferrite. This kind of structure is common, and examples of other austenite clusters that are likely to have sequential twinning are shown in Fig. 6.

The occurrence of twinned austenite particles explains why sometimes one may encounter intragranularly formed particles that do not appear to have any rational orientation relationship with the ferrite matrix. In the samples used in this study, some particles without apparent relationships were found. Since polishing sections each particle at a random plane, it should be quite normal that some austenite clusters would be sectioned in a plane that does not intersect the original nucleating crystal.

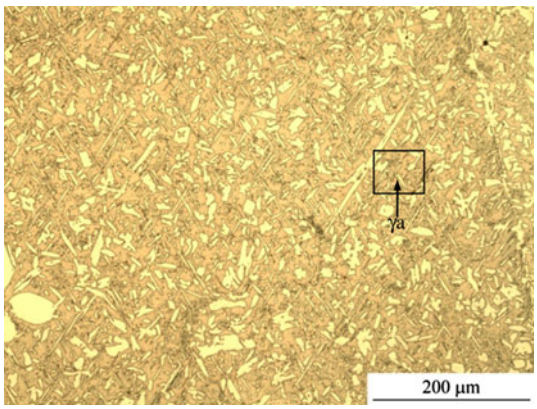

Fig. 7 Microstructure of a sample treated at 900 °C for 5,000 s

The microstructure of the sample treated at 900 °C for 5,000 s is shown in Fig. 7. Austenite growth took place in preferential directions, leading to a markedly acicular structure. This structure holds a remarkable resemblance to that of acicular ferrite as described by other authors [10–12]. Some clusters of sigma phase were also observed. However, the isothermal treatment caused complete nitride dissolution, and it is possible that nitrogen diffusion was also the controlling process for austenite formation during the isothermal hold at 900 °C. In the absence of pearlitic structures, acicular ferrite is known to improve the fracture toughness of carbon and low alloy steels. One may expect a similar effect from the formation of acicular austenite. However, the formation of sigma phase should have a negative influence on the impact toughness of duplex stainless steels, thus reducing the efficiency of the formation of acicular austenite in improving the mechanical properties of the material. Therefore, one may intuitively expect that the efficiency of acicular intragranular austenite in improving the mechanical properties depends deeply on the avoidance of brittle intermetallic phases such as sigma. Enbrittlement may be overcome by performing the isothermal treatment hold in conditions in which sigma formation does not occur (even at temperatures in which it *will* eventually take place). For example, Pohl and Storz [13] measured the kinetics of sigma formation in a similar steel. Sigma formation follows a C-curve, and the nose of the curve occurs at 850 °C. While sigma formation takes place after <1 h at 900 °C, it will take considerably longer at 950°, as that temperature already corresponds to the upper part of the C-curve for sigma transformation. Isothermal treatments performed by the authors at 1,000 °C caused no sigma formation at all, even for times as long as

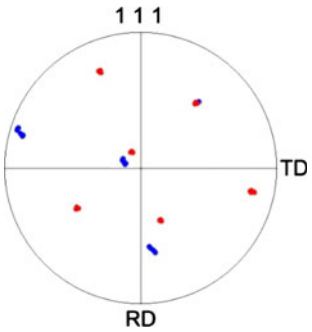

Fig. 8 Overlap of stereographic projections of γa (111 projection), labeled in Fig. 7, and the ferrite matrix (110 projection). There are two slightly deviated sets of austenite plane projections, indicating a small spread in the austenite orientation along the elongated particle

Table 4 Calculated orientation relationships between elongated austenite particles indicated in Fig. 8 and the ferrite matrix

Crystals	Orientation relationships	
γa/α	$(1\bar{1}1)\gamma \xrightarrow{1^\circ} (101)\alpha$	$[\bar{1}01]\gamma \xrightarrow{3^\circ} [\bar{1}\bar{1}1]\alpha$

15,000 s. The austenite particles remained elongated after treatment for 5,000 s, but some spheroidization and elimination of facets had begun to take place.

Crystallographic analysis using EBSD were also conducted on elongated austenite particles formed at 900 °C. One region, indicated in Fig. 7, was selected for EBSD analysis. The austenite particle chosen from the right end of Fig. 7, labeled γa, had a near exact planar relationship with the matrix, but a slight deviation from the Kurdjumov–Sachs relation conjugate direction. The graphical analysis of the orientation relationship between the γa and the ferrite matrix is shown in Fig. 8. The calculated orientation relationships between γa and α are shown in Table 4. It should be noticed, however, that the orientation of γa was slightly spread. The stereographic projection of γa has indeed two very close sets of plane projections. This is an indication that either sympathetic formation of austenite may have taken place during growth, with a slight deviation between the newly formed austenite and the particle that served as nucleation site, or that the austenite crystal may have undergone a deviation during growth. This was observed before by Shek et al. [4]. According to them, the orientation of Widmanstätten particles changes slightly during growth approaching the exact relationships toward the tip of the elongated particle. The "roots" of the Widmanstätten particles, on the other hand have a larger deviation from the exact ORs.

Shek et al. [4] observed the tendency toward an optimum deviation of 2.3° from the K–S relationship. This deviation is a way to achieve the best compromise between the atomic fit between planes and the maintenance of the invariant line during the transformation.

Conclusions

Early stages of intragranular austenite formation involves nucleation of a nucleus holding an OR followed by successive twinning events.

Intragranular austenite formed after isothermal treatments at 900 °C for 5,000 s has elongated shapes, very similar to acicular ferrite.

The orientation relationships between intragranular acicular austenite and the ferrite matrix are close to K–S with small deviations (close to 3°). These deviations are probably a compromise between keeping an atomic fit at the interphase boundaries and maintaining the invariant line during the transformation. No clear metallographic evidences of sympathetic nucleation were observed. Nevertheless, a spread in austenite orientation along a single elongated particle was noticed, and that may be a sign of sympathetic nucleation.

References

1. Snape E, Church NL (1972) J Met 24:23
2. Yokomiso T et al (2003) Mater Sci Eng A 344:261
3. Spanos G, Wilson AW, Kral MV (2005) Metall Mater Trans 36A:1209
4. Shek CH et al (2000) Metall Mater Trans 31A:15
5. Beraha E, Shpigler B (1977) Color metallography. ASM, Metals Park, p 160
6. Bunge HJ (1991) Steel Res 62(12):530
7. Monlevade EF, Falleiros IGS (2006) Metall Mater Trans 37A:939
8. Bieler TR et al (2006) In: 56th electronic components and technology conference (proceedings). IEEE, San Diego
9. Lehman LP et al (2004) J Electr Mater 33:1429
10. Madariaga I, Gutiérrez I, Bhadeshia HKDK (2001) Metall Mater Trans 32A:2187
11. Díaz-Fuentes M, Gutiérrez I (2003) Mater Sci Eng A 363:316
12. Pan T et al (2006) Mater Sci Eng A 438–440:1128
13. Pohl M, Storz O (2004) Z Metallk 95:631